Available online at www.sciencedirect.com
ScienceDirect
Catalysis Today 133–135 (2008) 925–930
CATALYSIS TODAY
www.elsevier.com/locate/cattod

Effect of aluminum on the properties of lanthana-supported nickel catalysts

S.P. de Lima [a], V. Vicentini [b], J.L.G. Fierro [c], M.C. Rangel [a,*]

[a] GECCAT Grupo de Estudo em Cinética e Catálise, Instituto de Química, Universidade Federal da Bahia, Campus Universitário de Ondina, Federação 40 170-290, Salvador, Bahia, Brazil
[b] Oxiteno S/A Indústria e Comércio, Avenida Ayrton Senna da Silva 3001, 09380-440 Mauá, São Paulo, Brazil
[c] Instituto de Catálisis y Petroleoquímica, CSIC, Cantoblanco, 28049 Madrid, Spain

Available online 21 February 2008

Abstract

The effect of aluminum addition on the properties of lanthanum oxide was investigated in order to find new supports for catalytic purposes. Pure lanthanum oxide and aluminum-loaded lanthanum oxide were prepared by precipitation techniques and impregnation with nickel salt. The supports and the catalysts were characterized by several techniques and the catalysts were evaluated in methane steam reforming, an important commercial route to produce high purity hydrogen. The results showed that aluminum changed the properties of lanthana-supported nickel catalysts improving the activity in methane steam reforming and the selectivity to hydrogen. The aluminum-free catalyst showed low activity since the first hours of reaction. On the other hand, the aluminum-loaded catalyst showed high activity and selectivity to hydrogen, which increased even more during reaction. This finding can be explained in terms of the production of metallic nickel, from the nickel compounds in strong interaction with the support. Therefore, the most promising catalyst was the aluminum-loaded lanthana, which showed high activity, selectivity to hydrogen and stability under reaction conditions.

Keywords: Steam methane reforming; Nickel; Lanthana; Hydrogen; Syngas

1. Introduction

The methane steam reforming is the main commercial route for producing hydrogen and synthesis gas ($CO + H_2$), important raw materials in several processes like ammonia and methanol synthesis, as well as in various petrochemical processes [1]. The synthesis gas (syngas) is also widely used in the Fischer–Tropsch reaction that consumes about 60% of its production worldwide. On the other hand, methane steam reforming produces 50% of the high purity hydrogen consumed all over the world, although this product can be also produced from naphtha steam reforming, from coal or from the electrolysis of the methane-based feeds [2,3].

In the steam reforming, light hydrocarbons react with steam, producing syngas (Eq. (1)), a process generally followed by water gas shift reaction, shown by Eq. (2) [4].

$$CH_4 + H_2O \rightleftarrows CO + 3H_2 \qquad \Delta H^{\circ}_{298} = 206.0\,\mathrm{kJ\,mol^{-1}} \quad (1)$$

$$CO + H_2O \rightleftarrows CO_2 + H_2 \qquad \Delta H^{\circ}_{298} = -41.2\,\mathrm{kJ\,mol^{-1}} \quad (2)$$

The methane steam reforming (MSR) is highly endothermic, therefore being favored by high temperature conditions. For this reason, the processes are industrially performed at 800 °C, pressure higher than 20 bar and a water-to-methane molar ratio in the range of 2.5–3.0 [2]. These severe operation conditions lead to several problems and determine the stability of the catalyst, which is mainly related to coke deposition [4–7]. Under these process conditions, coke is mainly produced by reactions shown by Eqs. (4) and (7).

$$CH_4 \rightarrow C + H_2 \quad (4)$$

$$2CO \rightarrow C + CO_2 \quad (5)$$

$$CO + H_2 \rightarrow C + H_2O \quad (6)$$

$$C_nH_{2n+2} \rightarrow nC + (n+1)H_2 \quad (7)$$

* Corresponding author.
E-mail address: mcarmov@ufba.br (M.C. Rangel).

0920-5861/$ – see front matter © 2008 Elsevier B.V. All rights reserved.
doi:10.1016/j.cattod.2007.12.065

In order to overcome the problem of coke deposition in the MSR, a tremendous body of work has been carried out, since the first commercial process operation. For many years nickel has been recognized as the most suitable catalyst for this process. Other metals such as rhodium, platinum, ruthenium and cobalt show high stability and selectivity towards hydrogen, especially rhodium which was also the most stable one [3,4]. The nickel-based catalysts usually show high activity and selectivity, but deactivate with time due to sintering and to coke deposition on the solid surface, that blocks the pores, impairing the reagents access to the active sites [7,8]. In this case, carbon is dissolved into the metal and diffuses through the metal–support interface, producing filaments that move the nickel particles away from the catalysts, causing the loss of the active phase of the steam reforming [9]. The noble metals are not able to dissolve carbon and then filamentous carbon is not produced [10,11]. In spite of these drawbacks, nickel is much cheaper than noble metals and thus is the only metal considered for industrial applications [12].

In industrial processes, coke deposition is controlled by adding an excess of steam to the reactor and using a catalytic support that can minimize carbon production. The most used commercial catalyst is constituted by nickel supported on a refractory material such as alumina (γ-Al_2O_3) with promoters, usually alkaline metal for improving the support stability and for suppressing the coke deposition [4,5].

As coke burning from spent catalyst is a highly exothermic reaction, which occurs at high temperature, the support must show not only a high thermal stability but also facilitate coke removal [10–13]. Several studies had shown that basic catalysts promote the reaction of carbon with steam, decreasing the coke deposition. Therefore, several basic systems have been studied either as promoters or as supports for nickel catalysts [14]. Among them, lanthana has been pointed out as a promising option because of its basicity and its high thermal stability [15]. In this context, this work aims to study the effect of aluminum on the properties of lanthana with the aim of finding alternative supports to MRS catalysts.

2. Experimental

2.1. Sample preparation

The samples with lanthanum-to-aluminum molar ratio of 10 (LA sample) were prepared by hydrolysis of aluminum and lanthanum nitrate, at room temperature. The sol produced was centrifuged and rinsed with water to remove the nitrate ions. The sample was calcined at 600 °C, for 4 h. Aluminum oxide (A sample) and lanthanum oxide (L sample) were also prepared by the same procedure. The supports were impregnated with a nickel nitrate solution at room temperature, in order to obtain a nickel catalyst 15% weight, and then calcined at the same conditions. The catalysts will be referred to hereafter as NA, NL and NLA.

2.2. Catalyst characterization

The supports and precursors were characterized by thermogravimetry, differential thermal analysis, Fourier transform infrared spectroscopy (FTIR), X-ray diffraction and specific surface area measurements. The catalysts were characterized by temperature-programmed reduction, energy dispersive X-ray spectroscopy, Fourier transform infrared spectroscopy, X-ray diffraction, specific surface area measurements and X-ray photoelectron spectroscopy (XPS). The spent catalysts were characterized by specific surface area measurements, X-ray diffraction, XPS and carbon measurements.

Thermogravimetric (TG) and differential thermal analysis (DTA) were performed using a Mettler-Toledo model SDTA 851 equipment. The samples (0.015 g) were heated from room temperature up to 1000 °C, at a rate of 10 °C min^{-1}, under air flow (50 mL min^{-1}). The elemental analysis of the catalysts was carried out by energy dispersive X-ray spectroscopy using a Shimadzu model EDX 700HS instrument in helium atmosphere.

X-ray diffraction patterns were recorded at room temperature in a Shimadzu model XRD 6000 equipment. The experiments were carried out by using nickel filter and Cu Kα (λ = 1.54051 A) radiation generated at 40 kV and 30 mA. The specific surface areas (Sg) were measured in a Micromeritics ASAP 2020 instrument. The catalyst (0.25 g) was activated by heating at 200 °C for 1 h, under vacuum (10^{-6} mbar). Nitrogen adsorption experiments were carried out at 77 K.

In order to obtain the temperature-programmed reduction profile, a Micromeritics model TPD/TPR 2900 equipment was used. Samples (0.25–0.3 g) were reduced in a range from 30 to 600 °C, at 10 °C min^{-1}, under a 5% H_2/N_2 mixture flow. The carbon content in the spent samples was determined in a Leco model CS-200 equipment, using Lecocel and the iron chip accelerator.

Photoelectron spectra (XPS) were obtained in a VG Escalab 200R spectrometer using a hemispherical electron analyser and Mg Kα X-ray source. The powder samples were pressed in a copper holder, which was introduced in the pre-treatment chamber, where the sample was degassed to 350 °C for 1 h, before being introduced in the analysis chamber. Peak intensities were estimated by calculating the integral of each peak after smoothing and subtraction of an S-shaped background and fitting the experimental peak by a least-squares routine using Gaussian and Lorentzian lines. Atomic ratios were computed from the intensity ratios normalized by atomic sensitivity factors. The binding energy (BE) reference was taken at the C 1s peak from carbon contamination of the samples at 284.9 eV, which gives a precision of $\pm$0.2 eV.

2.3. Catalytic tests

The catalysts were evaluated in a stainless steel microreactor using samples (0.15 g) previously reduced *in situ* under hydrogen flow at 500 °C for 2 h. The reaction was carried out at 600 °C, 1 bar and using a steam-to-methane molar ratio

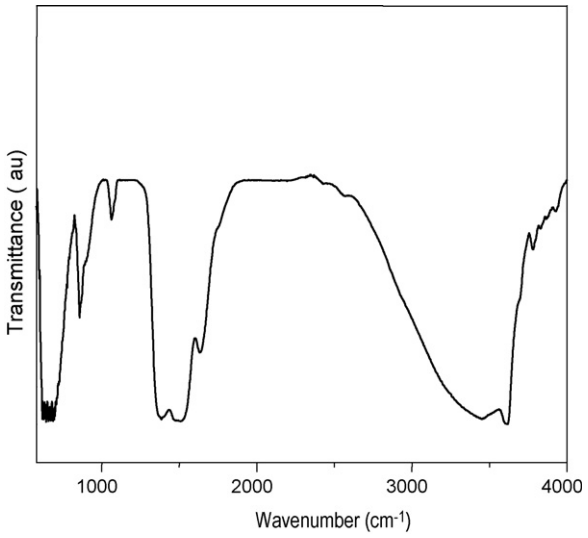

Fig. 1. Fourier transform infrared spectrum of calcined lanthana (L sample).

of 4. A mixture of 10% methane in nitrogen was fed to a saturator with water, kept at 80 °C, and then fed to the reactor. Each run took 6 h and the products were analyzed in a Thermo Fennigan model Trace GC chromatograph equipped with thermal conductivity and flame ionization detectors.

3. Results and discussion

The FTIR spectra of the catalysts and supports showed characteristic bands of nitrate species at 1389 cm^{-1} [16], indicating that the rinsing and calcination processes were not enough for the removal of those anion salt precursors from the solids. Fig. 1 presents the typical pattern of the spectra.

The thermogravimetry curves of the supports are shown in Fig. 2(a). In all cases, a weight loss was observed below 100 °C, attributed to the loss of water and of volatiles, which were adsorbed on solids. This event was confirmed by the differential thermal analysis curves, which presented an endothermic peak at this temperature range. It was noted a weight loss with a maximum at 250, 300 and 380 °C for the A, L and LA samples, respectively, assigned to the removal of residual nitrate salt precursor species, as well as to the removal of hydroxyl groups. A second weight loss, taking place at higher temperatures, with a maximum at 420, 500 and 600 °C for the A, L and LA samples, respectively, is related to metallic oxide formation [13]. These events were confirmed by differential thermal analysis, which showed three endothermic peaks in the same temperature range.

The thermogravimetric profiles of the catalysts (Fig. 2(b)), showed two weight losses: the first one at 100 °C is attributed to the loss of volatiles and the second one, within the range of 350–420 °C, is associated to decomposition of nickel nitrate into the corresponding nickel oxide.

Fig. 3 (a) presents the X-ray diffraction patterns of the supports. Pure alumina (A sample), showed only peaks of alumina, γ-Al_2O_3 (JCPDS 48-0367), while pure lanthanum-based sample (L) showed diffraction lines of lanthana, La_2O_3 (JCPDS 05-0602) and of the orthorhombic lanthanum nitrate

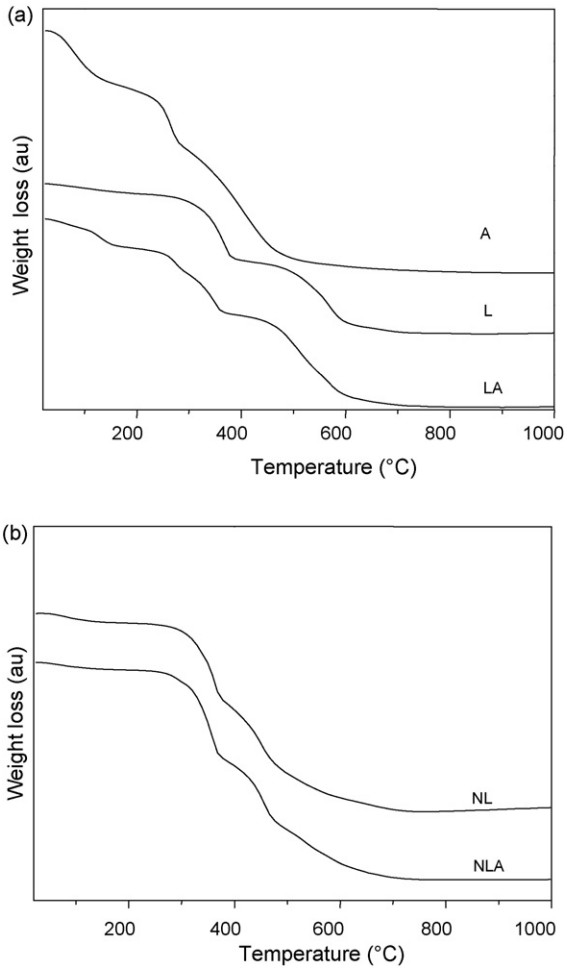

Fig. 2. Thermogravimetry curves of (a) support precursors and of (b) catalyst precursors. A, L and LA samples: alumina, lanthana and aluminum-loaded lanthana. N represents nickel.

hydroxide, $La(OH)_2NO_3$ (JCPDS 26-1144). The addition of small amounts of aluminum to lanthana avoided the production of lanthana nitrate hydroxide and then only lanthanum oxide was detected. Therefore, the removal of nitrate species was easier in this solid.

X-ray diffraction patterns of the fresh catalysts are shown in Fig. 3 (b). In both cases, lanthana (JCPDS 05-0602) and lanthanum nickel oxide, La_2NiO_4 (JCPDS 86-1668) were detected. In the aluminum-free sample, nickel oxide, NiO (JCPDS 85-1977) was also observed. During reaction, metallic nickel (JCPDS 03-1051) was produced, regardless the presence of aluminum, as shown in Fig. 4. It can be also noted that nickel interacted with lanthana during reaction produced a more crystallized lanthanum nickel oxide as compared to fresh catalyst.

The specific surface area of lanthana decreased due to aluminum as shown in Table 1, indicating that aluminum did not improve the textural properties of this solid. After nickel impregnation, the solids showed similar specific BET areas. Spent catalysts showed especific surface area lower than the fresh catalysts (Table 2).

The temperature-programmed reduction profiles of the samples are shown in Fig. 5 (a). As was expected, A sample did

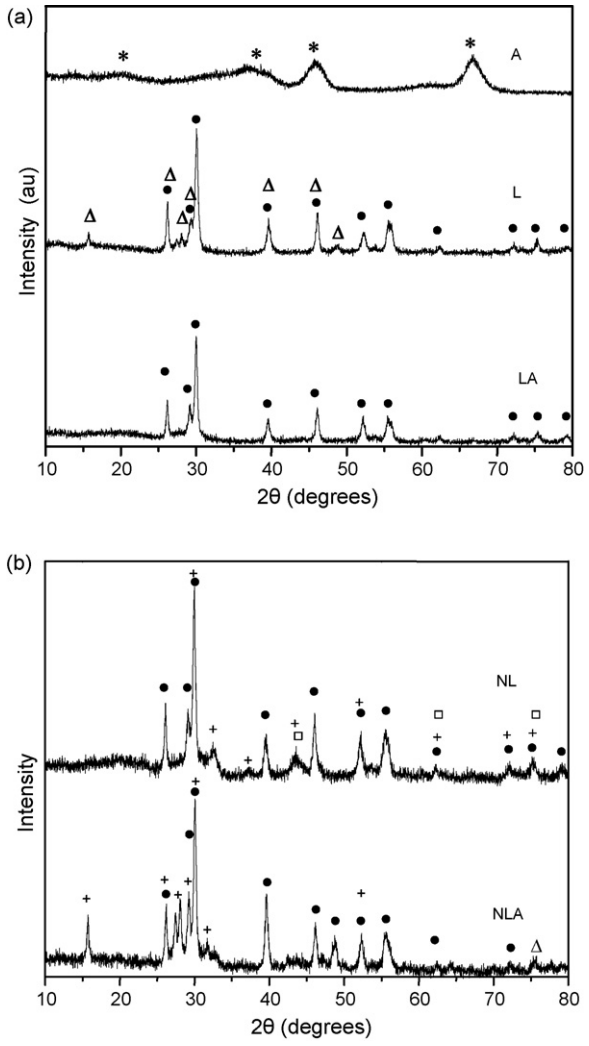

Fig. 3. Diffractograms of (a) the supports and of (b) the catalysts. A, L and LA samples: alumina, lanthana and aluminum-loaded lanthana. N represents nickel. (Δ) $La(OH)_2NO_3$; (*) γ-Al_2O_3; (●) La_2O_3; (□) NiO; (+) La_2NiO_4.

not show any peak, since alumina cannot be reduced at temperatures lower than 1000 °C [17]. For the other samples, the curves showed several reduction peaks, which can be attributed to the reduction of nitrate species in different stages as well as to lanthana reduction [18–20]. The presence of these species was detected by FTIR and X-ray diffraction. On the other hand, the curves of the catalysts, shown in Fig. 5 (b), displayed different profiles. The aluminum-free sample showed peaks at 230, 360 and 530 °C. The first one can be assigned to the reduction of segregated nickel oxide (NiO) and of nitrate

Table 1
Specific surface area (Sg) of the supports and of the fresh catalysts. L and LA samples: lanthana and aluminum-loaded lanthana, respectively. N represents nickel

Sample	Sg ($m^2\ g^{-1}$)
L	35
LA	22
NL	19
NLA	18

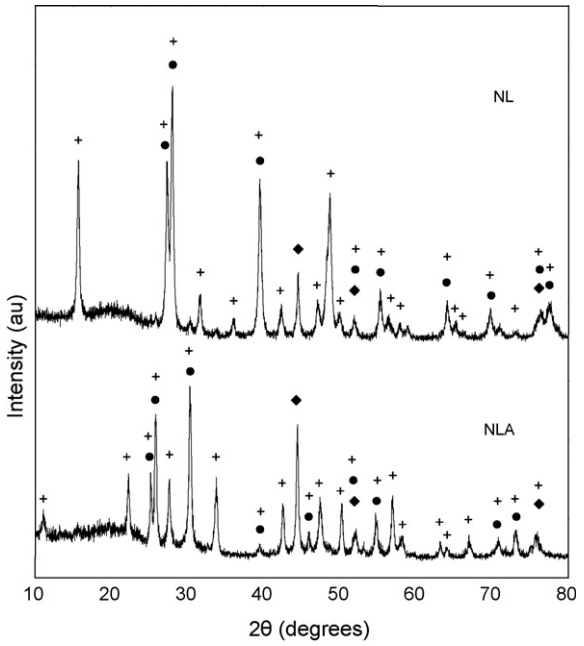

Fig. 4. Diffractograms of the spent catalysts. NL and NLA samples: nickel supported in lanthana and aluminum-loaded lanthana. (●) La_2O_3; (+) La_2NiO_4; (◆) Ni.

species, detected by thermal analysis and FTIR. The second peak can be due to the reduction of nickel oxide species (NiO) in weak interaction with the support while the third one can be associated to the reduction of nickel species strongly interacting with the support [13,18]. In a similar way, the aluminum-doped lanthana (NLA sample) also showed three reduction peaks at 280, 520 and 800 °C. As no diffraction peak of nickel oxide was observed for this sample, it is inferred that these three H_2-consumption peaks belong to reduction of highly dispersed Ni^{2+} ions on the surface of NLA substrate. By comparing the reduction profiles of NL and NLA samples, it can be observed that the peaks were shifted to higher temperatures due to aluminum incorporation, indicating that aluminum oxide makes the reduction of Ni^{2+} species more difficult. The shift of the high temperature peak to 800 °C suggests the formation of nickel aluminate ($NiAl_2O_4$) [14], although it must be highly dispersed since it cannot be detected by X-ray diffraction. In addition, the strong overlapping of diffraction lines of $NiLa_2O_4$ phase and that of the Al_2O_3 makes difficult, if not impossible, its detection by diffraction methodology.

The binding energy (BE) Al 2p, C 1s, La $3d_{5/2}$, Ni $2p_{3/2}$ and O 1s core-levels of the samples are compiled in Table 3. For C 1s core-level peak around 289.3 eV is typical of carbonate species [21] while that of Al 2p comes from Al_2O_3 phase. This

Table 2
Specific surface area (Sg*) and carbon content of the spent (S) catalysts. NL and NLA samples: nickel supported on lanthana and on aluminum-loaded lanthana, respectively

Sample	NL-S	NLA-S
Sg ($m^2\ g^{-1}$)	11	5
Carbon content (%)	0.23	1.05

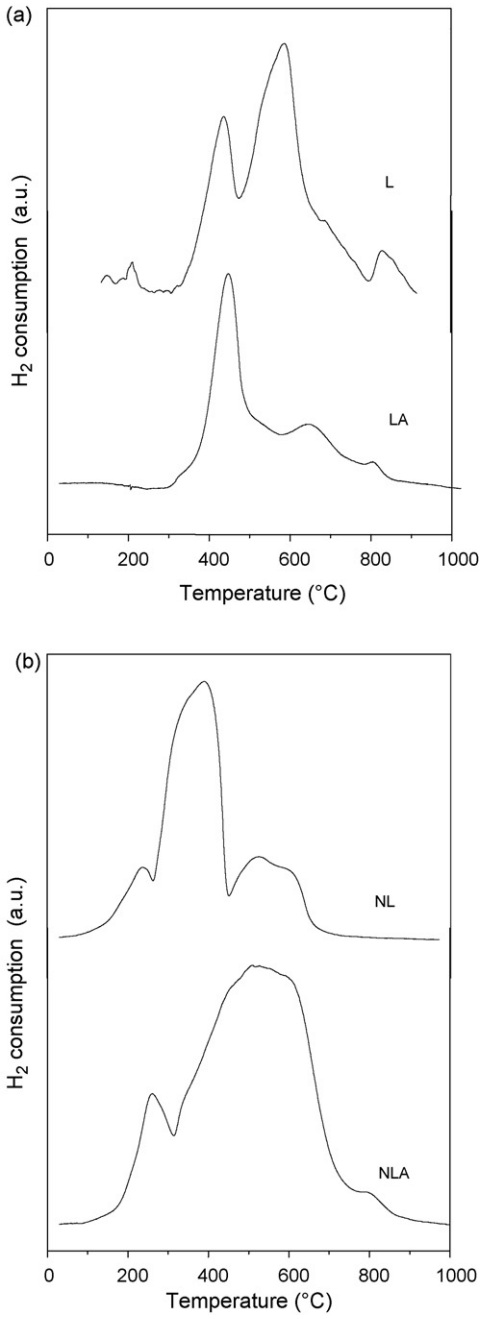

Fig. 5. Temperature-programmed reduction of (a) the supports and of (b) the catalysts. A, L and LA samples: alumina, lanthana and aluminum-loaded lanthana, respectively; N represents nickel.

because La_2O_3 is a basic oxide which is easily carbonated by exposure to ambient atmosphere. The Ni 2p profile is complex due to overlapping of Ni 2p and La 3d peaks. The most intense Ni $2p_{3/2}$ peak, which appears at around 855.5 eV, is characteristic of Ni^{2+} ions in an oxygen environment and is accompanied by a satellite line positioned at ca. 6 eV on the higher BE side. This satellite is fingerprint of Ni^{2+} ions. The Ni 2p peaks are complicated by the simultaneous presence of La $3d_{3/2}$ component ca. 4 eV lower BE. The La 3d spectra show the doublets corresponding to spin–orbit ($3d_{5/2}$, $3d_{3/2}$) coupling phenomena with peaks at 834.8 and 852.7 eV, typical of La_2O_3, as well as to the splitting due to hybridization phenomena of the

Table 3
Binding energies (eV) of core-levels of the samples before and after (S) the methane steam reforming. NL and NLA samples: nickel supported on lanthana and on aluminum-loaded lanthana, respectively

Sample	C 1s	La $3d_{5/2}$	O 1s	Al 2p	Ni $2p_{1/2}$
NL	289.5	834.6	531.0	–	872.5
NLA	289.4	835.0	531.4	74.4	873.1
NLA-S	289.6	835.0	531.6	74.5	872.9

Table 4
Atomic surface composition of fresh and spent (S) catalysts. NL and NLA samples: nickel supported on lanthana and on aluminum-loaded lanthana, respectively

Sample	Ni/La	Al/La	Ni/Al	Ni/(Al + La)	CO_3^{2-}/La
NL	0.699	–	–	0.699	0.992
NLA	0.122	0.249	0.481	0.097	0.694
NLA-S	0.078	0.240	0.326	0.063	1.116

$3d^94f^1$ and $3d^94f^0$ final states, respectively, in case of La $3d_{5/2}$ line [22]. Thus, the higher BE contribution of the La $3d_{3/2}$ peak overlaps with the Ni $2p_{3/2}$ peak, which masks not only the accurate measure of the BE of nickel but also its intensity. To

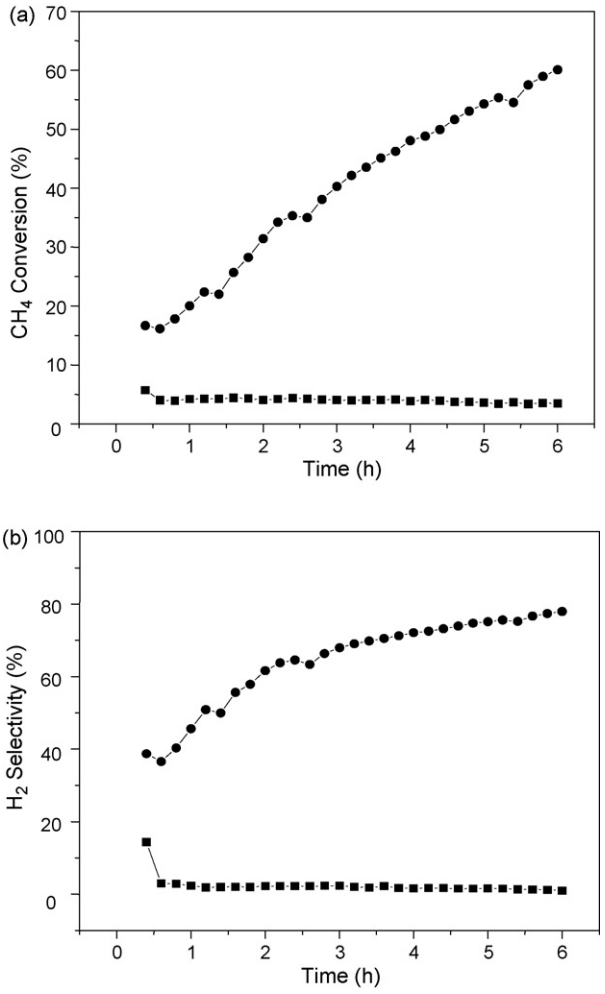

Fig. 6. (a) Methane conversion over catalysts produced and (b) hydrogen selectivity. NL and NLA samples: nickel supported on lanthana (■) and on aluminum-loaded lanthana (●), respectively.

overcome this complication, the BE of the less intense Ni $2p_{1/2}$ peak was measured. The BE values at 872.7.873.2 eV reveal the presence of ionic nickel species.

From the intensities of Al 2p, La $3d_{5/2}$, C 1s and Ni $2p_{1/2}$ peaks and considering the sensitivity factors given by Wagner et al. [23], the Ni/Al, Al/La, Ni/(Al + La) and CO_3^{2-}/La atomic ratios were calculated. These ratios are also compiled in Table 4. It can be noted that the surface of the aluminum-free sample is richer is nickel than the aluminum-loaded lanthanum oxide. In addition, nickel migrated from the surface during reaction.

All catalysts were active in the MSR reaction and selective to hydrogen, as is illustrated in Fig. 6. The aluminum-free sample led to low conversions since the beginning of reaction. The selectivity to hydrogen as a function of reaction time showed the same profile, reaching values close to 2% at the end of reaction. On the other hand, the aluminum-loaded lanthana (NLA sample) led to high conversion values (30%), at the beginning of reaction. A further increasing of around 60% was achieved after 6 h of reaction time. The selectivity curve presented a similar profile, showing selectivity to hydrogen of about 30% at the beginning of the reaction and 70% after 5 h of reaction time. The activity increased probably due to an increase of the metallic sites during reaction, which are selective to hydrogen production. These sites come likely from the slow reduction (by the hydrogen generated in the SMR reaction) of a fraction of the $NiAl_2O_4$ phase formed during air-calcination of the impregnate precursor. As noted by temperature-programmed reduction, the presence of aluminum makes the nickel reduction more difficult. All catalysts showed low amounts of coke as shown in Table 2.

4. Conclusions

The addition of aluminum to lanthana, by simultaneous hydrolysis of the corresponding metallic nitrate, followed by calcination, leads to structural and textural changes of lanthana. The lanthana support is made of lanthanum oxide and lanthanum nitrate hydroxide while the aluminum-loaded support contains only lanthanum oxide. The nickel incorporated to the lanthana substrate forms not only nickel oxide (NiO) but also La_2NiO_4 phase via solid-state reaction with La_2O_3 while nickel incorporated onto Al-loaded La_2O_3 develops a stable, difficult to reduce $NiAl_2O_4$ phase.

All activated catalysts were active in the MSR reaction and were selective to hydrogen, but the aluminum-free one showed very low activity. On the other hand, the aluminum-loaded catalyst led to high methane conversion and showed high selectivity to hydrogen; both increasing during reaction. This can be assigned to reduction of the nickel phases in strong interaction with support, by the hydrogen produced in the reaction.

Briefly, aluminum changes the textural and chemical properties of lanthana-supported nickel improving its catalytic performance, such as activity, selectivity to hydrogen and stability.

Acknowledgements

SPL thanks CAPES for her graduate scholarship. The authors thank CNPq and FINEP for the financial support.

References

[1] A.M. Adris, C.J. Limm, J.R. Grace, Chem. Eng. Sci. 52 (1997) 1609.
[2] J.N. Armor, Appl. Catal A: Gen. 176 (1999) 159.
[3] N. Sittichai, O. Oktar, U.S. Ozkan, J. Mol. Catal. A: Chem. 241 (2005) 133.
[4] Y. Wang, Y.H. Chin, R.T. Rozmiarek, B.R. Johnson, Y. Gao, J. Watson, A.Y.L. Tonkovich, D.P. van der Wiel, Catal. Today 98 (2005) 575.
[5] A.F. Lucrédio, E.M. Assaf, J. Power Sources 159 (2006) 667.
[6] J.S. Lisboa, D.C.R.M. Santos, F.B. Passos, F.B. Noronha, Catal. Today 101 (2005) 15.
[7] Q. Miao, G. Xiong, S. Sheng, W. Cui, L. Xu, X. Guo, Appl. Catal. A: Gen. 154 (1997) 17.
[8] R. Jin, Y. Chen, W. Li, W. Cui, Y. Ji, C. Yu, Y. Jiang, Appl. Catal. A: Gen. 201 (2000) 71.
[9] T. Sperle, D. Chen, R. Lodeng, A. Holmen, Appl. Catal. A: Gen. 282 (2005) 195.
[10] J.A.C. Dias, J.M. Assaf, J. Power Sources 137 (2004) 264.
[11] D.L. Trimm, Catal. Today 49 (1999) 3.
[12] M.A. Peña, J.P. Gómez, J.L.G. Fierro, Appl. Catal. A: Gen. 144 (1996) 7.
[13] B. Ersoy, V. Gunay, Ceram. Int. 30 (2004) 163.
[14] E. Ruckenstein, Y.H. Hu, J. Catal. 161 (1996) 55.
[15] S. Kus, M. Otremba, M. Taniewski, Fuel 82 (2003) 1331.
[16] R.A. Niquist, R.O. Kagel, Infrared Spectra of Inorganic Compounds, Academic Press, Orlando, 1971, p. 3.
[17] J. Wang, L. Dong, Y. Hu, G. Zheng, Z. Hu, Y. Chen, J. Solid State Chem. 157 (2001) 274.
[18] A.A. Lemonidou, I.A. Vasalos, Appl. Catal. A: Gen. 228 (2002) 227.
[19] S. Ho, T. Chou, Ind. Eng. Chem. Res. 34 (1995) 2279.
[20] A. Jones, B. McNicol, Temperature-Programmed Reduction for Solid Materials Characterization, Marcel Dekker Inc., New York, 1986.
[21] J.L.G. Fierro, Catal. Today 8 (1990) 153.
[22] A.N. Chaika, A.M. Ionov, N.A. Tulina, D.A. Shulyatev, Ya.M. Mukovskii, J. Elect. Spec. Relat. Phenom. 148 (2005) 101.
[23] C.D. Wagner, L.E. Davis, M.V. Zeller, J.A. Taylor, R.H. Raymond, L.H. Gale, Surf. Interf. Anal. 3 (1981) 211.